NeuroImage: Clinical 31 (2021) 102678

Contents lists available at ScienceDirect

NeuroImage: Clinical

journal homepage: www.elsevier.com/locate/ynicl

Myelination may be impaired in neonates following birth asphyxia

Bianca Olivieri [a], Emmanouil Rampakakis [b,c], Guillaume Gilbert [d], Aliona Fezoua [a], Pia Wintermark [a,e,*]

[a] Research Institute of the McGill University Health Centre, McGill University, Montreal, QC, Canada
[b] Medical Affairs, JSS Medical Research, Montreal, Québec, Canada
[c] Department of Pediatrics, Montreal Children's Hospital, McGill University, Montreal, QC, Canada
[d] MR Clinical Science, Philips Healthcare, Montreal, QC, Canada
[e] Department of Pediatrics, Division of Newborn Medicine, Montreal Children's Hospital, McGill University, Montreal, QC, Canada

ARTICLE INFO

Keywords:
Asphyxia
Brain
Hypothermia
Magnetic resonance imaging
Myelination
Neonate
Neonatal encephalopathy

ABSTRACT

Background: Myelination is a developmental process that begins during the end of gestation, intensifies after birth over the first years of life, and continues well into adolescence. Any event leading to brain injury around the time of birth and during the perinatal period, such as birth asphyxia, may impair this critical process. Currently, the impact of such brain injury related to birth asphyxia on the myelination process is unknown.

Objective: To assess the myelination pattern over the first month of life in neonates with neonatal encephalopathy (NE) developing brain injury, compared to neonates without injury (i.e., healthy neonates and neonates with NE who do not develop brain injury).

Methods: Brain magnetic resonance imaging (MRI) was performed around day of life 2, 10, and 30 in healthy neonates and near-term/term neonates with NE who were treated with hypothermia. We evaluated myelination in various regions of interest using a T2* mapping sequence. In each region of interest, we compared the T2* values of the neonates with NE with brain injury to the values of the neonates without injury, according to the MRI timing, by using a repeated measures generalized linear mixed model.

Results: We obtained 74 MRI scans over the first month of life for 6 healthy neonates, 17 neonates with NE who were treated with hypothermia and did not develop brain injury, and 16 neonates with NE who were treated with hypothermia and developed brain injury. The T2* values significantly increased in the neonates with NE who developed injury in the posterior limbs of the internal capsule (day 2: $p < 0.001$; day 10: $p < 0.001$; and day 30: $p < 0.001$), the thalami (day 2: $p = 0.001$; day 10: $p = 0.006$; and day 30: $p = 0.016$), the lentiform nuclei (day 2: $p = 0.005$), the anterior white matter (day 2: $p = 0.002$; day 10: $p = 0.006$; and day 30: $p = 0.002$), the posterior white matter (day 2: $p = 0.001$; day 10: $p = 0.008$; and day 30: $p = 0.03$), the genu of the corpus callosum (day 2: $p = 0.01$; and day 10: $p = 0.006$), and the optic radiations (day 30: $p < 0.001$).

Conclusion: In the neonates with NE who were treated with hypothermia and developed brain injury, birth asphyxia impaired myelination in the regions that are myelinated at birth or soon after birth (the posterior limbs of internal capsule, the thalami, and the lentiform nuclei), in the regions where the myelination process begins only after the perinatal period (optic radiations), and in the regions where this process does not occur until months after birth (anterior/posterior white matter), which suggests that birth asphyxia, in addition to causing the previously well-described direct injury to the brain, may impair myelination.

Abbreviations: BI, brain injury; DOL, day of life; DTI, diffusion-tensor imaging; FOV, field of view; ihMT, inhomogenous magnetisation transfer; McDESPOT, multi-component driven equilibrium single pulse observation of T1 and T2; MCR, multicomponent relaxation; MR, magnetic resonance; MRI, magnetic resonance imaging; MRT, magnetisation transfer ratio; MWF, myelin water fraction; MWI, myelin water imaging; NBI, no brain injury; NE, neonatal encephalopathy; PLIC, posterior limb of the internal capsule; qMT, quantitative magnetisation transfer; SAR, specific absorption rate; SD, standard deviation; SNR, signal-to-noise ratio; TE, time to echo; TR, repetition time; TSE, turbo spin echo.

* Corresponding author at: McGill University/Montreal Children's Hospital, Division of Newborn Medicine, Research Institute of the McGill University Health Centre, 1001 boul. Décarie, Site Glen Block E, EM0.3244, Montréal, QC H4A 3J1, Canada.
E-mail address: pia.wintermark@gmail.com (P. Wintermark).

https://doi.org/10.1016/j.nicl.2021.102678
Received 1 January 2021; Received in revised form 17 March 2021; Accepted 12 April 2021
Available online 22 April 2021

1. Introduction

Myelination refers to the development of a protein-lipid bilayer that surrounds axons in the brain (Yeung et al., 2014). Myelin, produced by the glial cells of the nervous system, provides insulating support to axons, which enables the more efficient and specialized functioning of the brain (Saab et al., 2013; Yeung et al., 2014). The myelination phase represents the last steps of brain formation after synaptogenesis, and it is the only brain formation phase that occurs mostly after birth (Yeung et al., 2014). Impairment of the myelination process is known to disturb motor and sensory functions, and to cause cognitive impairments (Gold et al., 2012; Nave and Bruce, 2008; Saab et al., 2013). To date, most studies investigating brain myelination have been based on histopathological studies of fetuses', neonates', and infants' brains (Brody et al., 1987; Gilles, 1976; Hasegawa et al., 1992; Kinney et al., 1988). However, newly developed techniques of magnetic resonance imaging (MRI) have demonstrated their capacity to assess myelination in the brains of adults and children older than 3 months of age (Barkovich et al., 1998; Dean et al., 2016; Deoni et al., 2011, 2012; Huntenburg et al., 2017; Ning et al., 2014). Nevertheless, to date, these techniques have not been used widely to study the brains of neonates under 3 months of age or the brains of critically ill neonates.

Myelination is a progressive process that begins shortly before a term neonate is born, peaks after birth during the first years of life, and continues to be refined into adolescence (Yeung et al., 2014). Myelination continues into the second decade of life and beyond (Ding et al., 2008; Holland et al., 1986; O'Rahilly et al., 1999). Typically, myelination proceeds from the posterior to anterior regions of the brain, and from the central to peripheral regions of the brain (Barkovich and Hallam, 1997; Grodd, 1993). Since the myelination process peaks after birth during the first years of life, any event leading to brain injury that occurs around the time of birth and during the perinatal period may impair this process and thus worsen later neurodevelopmental impairments. An example of such an event is birth asphyxia, which is responsible for approximately 23% of all neonatal deaths worldwide (Al-Macki et al., 2009; Bryce, 2005; Cabaj et al., 2012; Fatemi et al., 2009; Ferriero, 2004), and which causes devastating long-term neurological complications such as cerebral palsy and cognitive delay (Barkovich et al., 1998; Huang & Castillo, 2008; Wang et al., 2008). Although the patterns of brain injury of neonates with neonatal encephalopathy (NE) have been well studied by MRI, the impact of such brain injury on myelination processes has not yet been researched. It is important to understand how birth asphyxia may impact myelination, since myelination impairment may contribute to later neurodevelopmental impairments. We have hypothesized that brain injury secondary to birth asphyxia impairs typical brain myelination processes. Thus, this study was designed to investigate brain myelination over the first month of life in healthy neonates and neonates with NE by using T2* mapping where higher T2* values reflect lower myelin content and lower T2* values reflect higher myelin content. In various studies, T2* values have been shown to correlate with myelin content (Baxan et al., 2010; Henkelman et al., 1993; Kucharczyk et al., 1994; Lee et al., 2012; Liu et al., 2011; Ning et al., 2014; O'Brien and Sampson, 1965; Stanisz et al., 1999; Zhong et al., 2011). However, although myelin may be the major contributing factor to the T2* measurements (Baxan et al., 2010; Kucharczyk et al., 1994; Stanisz et al., 1999; Henkelman et al., 1993; Lee et al., 2012; Liu et al., 2011; Ning et al., 2014; O'Brien and Sampson, 1965; Zhong et al., 2011), it may not be the only one. In adults, calcium depositions, iron content, and haemorrhagic infarcts have been shown to influence these measurements. Nevertheless, the neonatal brain is less likely to have a high concentration of iron and calcium, and thus myelin is probably the main contributor to the T2* values in the neonatal brain. In addition, this MR imaging technique has the advantage of a good signal-to-noise ratio (SNR) and a short scanning time of<4 min (Hwang et al., 2010), and thus can be added easily to the baseline protocol for imaging healthy and critically ill neonates.

2. Material and methods

2.1. Patients

We conducted a prospective cohort study of near-term/term neonates with NE who were admitted to our neonatal intensive care unit between 2014 and 2018, and who met the criteria for induced hypothermia: (1) gestational age $\geq$ 36 weeks and birth weight $\geq$ 1800 g, (2) evidence of fetal distress (e.g., a history of acute perinatal event, cord pH $\leq$ 7.0, or base deficit $\leq$ -16 mEq/L), (3) evidence of neonatal distress, such as an Apgar score $\leq$ 5 at 10 min, postnatal blood gas pH within the first hour of life $\leq$ 7.0 or base deficit $\leq$ -16 mEq/L, or a continuous need for ventilation initiated at birth and continued for at least 10 min, and (4) evidence of moderate or severe encephalopathy obtained by a standardized neurological exam and/or by an amplitude-integrated electroencephalogram. The eligible neonates received whole-body cooling to an esophageal temperature of 33.5 °C, initiated by 6 h of life and continued for 72 h. Healthy term neonates also were enrolled from the normal nursery and served as controls. The research protocol was approved by the institutional ethics review board, and we obtained informed parental consent for each case.

2.2. Brain magnetic resonance imaging (MRI)

As per the standard clinical protocol at our institution, we performed a brain MRI on all the neonates with NE after their hypothermia treatment was completed, typically around day 10 of life. In addition, when possible (i.e., when parents gave their consent to have additional MRIs performed on their neonates, when the neonates were hemodynamically stable, and when a team of a nurse and a respiratory therapist was available to go to the MRI), neonates underwent additional MRI scans on day 2 of life and around 1 month of age. We chose these time-points to assess early patterns of injury (day 2 of life) and to define the extent of definitive brain injuries (around 1 month of life). Neonates were wrapped with one or two thin blankets and placed on a Vac-Fix® MRI-compatible pillow containing small polystyrene spheres; they were fed before the MRI exam if they were not nihil per os at the time of the MRI (e.g., during therapeutic hypothermia). The neonates who were receiving hypothermia had their therapy maintained during the MRI scan, as previously described (Wintermark et al., 2010). Any ventilation, pressor support, or sedation was maintained during the MRI scanning process, and additional sedation was avoided. Regarding the healthy term neonates, we performed an MRI, if the parents consented, around day 10 of life or 1 month of life.

We performed the MRI scans using a 3 T clinical system (Achieva X; Philips Healthcare, Best, The Netherlands) with a 32-channel receive-only head coil (Philips). Each MRI imaging study included a 3D T1-weighted gradient echo (TR = 24 ms; TE = 4.6 ms; matrix size = 180 X 180; FOV = 180 mm; flip angle = 30°; sagittal sections = 104; section thickness = 1.0 mm; and multiplanar reformations in axial and coronal planes) and a high-resolution turbo spin echo (TSE) T2-weighted imaging (TR = 5000 ms; TE = 90 ms; TSE factor = 15; matrix size = 300 X 300; FOV = 150 mm; flip angle = 90°; axial sections = 27; section thickness = 3.0 mm). In addition, to assess the myelination of the enrolled neonates (Baxan et al., 2010; Henkelman et al., 1993; Kucharczyk et al., 1994; Lee et al., 2012; Liu et al., 2011; Ning et al., 2014; O'Brien and Sampson, 1965; Stanisz et al., 1999; Zhong et al., 2011), we performed a T2* mapping sequence consisting of a 3D multi-echo gradient-echo sequence (TR = 58 ms; 6 echoes with TE = 5 ms, 15 ms, 25 ms, 35 ms, 45 ms and 55 ms; matrix size = 256 × 200; FOV = 200 × 160 mm, flip angle = 15°, axial sections = 48; section thickness = 2 mm).

Pediatric neuroradiologists, who were blind to the clinical conditions of the infants, interpreted the conventional imaging (T1- and T2-weighted imaging) and diffusion-weighted imaging of the MRI scans performed on healthy neonates and neonates with NE, and reported the

presence and extent of brain injury according to a previously described MRI scoring system (Barkovich et al., 1998). We used the MRI scores obtained around day 10 of life as a reference to determine the extent of brain injury for each neonate (Boudes et al., 2015; Al Amrani et al., 2018).

2.3. T2* Mapping

We calculated and generated the T2* mapping on a voxel by voxel basis using the MRI console application software (Philips Healthcare, software releases R3.2 and R5.3), by assuming a mono-exponential decay of the magnitude of the signal as a function of the echo time and a maximum likelihood estimation approach. Registration was not possible, since the echoes are acquired in an interleaved manner; there was no bulk motion between the echoes.. We then manually performed the T2* measurements by using the Philips DICOM Viewer software version R3.0 (https://www.philips.com/c-dam/b2bhc/master/sites/netforum/Philips_DICOM_Viewer_-_download_version_R3.0_SP15.pdf) in eight regions of interest: i.e., the posterior limb of the internal capsule, the thalamus, the lentiform nucleus, the anterior and posterior white matter, the genu and splenium of the corpus callosum, and the optic radiations. The same observer who was blind to the presence or absence of brain injury obtained the measurements for our different regions of interest. This observer obtained measurements for the right and left sides of the regions of interest, except for the corpus callosum for which only one measurement was obtained. The observer took the measurements twice, to increase their reproducibility and robustness, and then averaged them.

2.4. Statistical analysis

For each region of interest, a separate repeated measures generalized linear mixed model was built to compare the T2* values of the neonates with injury and the neonates without brain injury. The neonates without injury included healthy neonates and neonates with NE who did not develop brain injury. Considering that the near-term/term neonates with NE treated with hypothermia may have a gestational age ranging between 36 and 42 weeks, and that the gestational age and the post-menstrual age at the time of the MRI may impact myelination, we included brain injury within the region of interest and its two-way interaction with day of life as fixed factors, and the gestational age as a covariate. To account for sequential multiple comparisons, we used a Sidak correction.

Finally, using Spearman's correlation, we explored the association between the T2* values and the post-menstrual gestational age at the time of the brain MRI scans. Given the exploratory nature of this

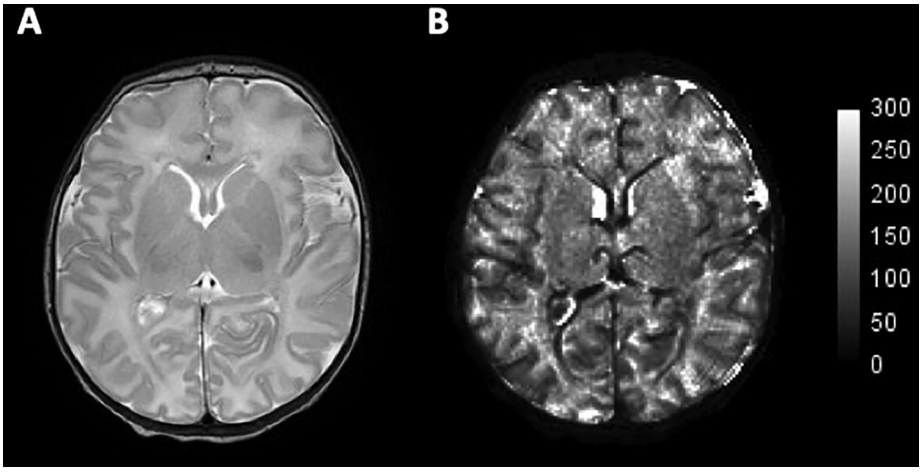

Fig. 1. (A) Axial T2-weighted imaging and (B) axial T2* map (ms) of a neonate with NE treated with hypothermia without brain injury on the brain MRI performed on day 11 of life.

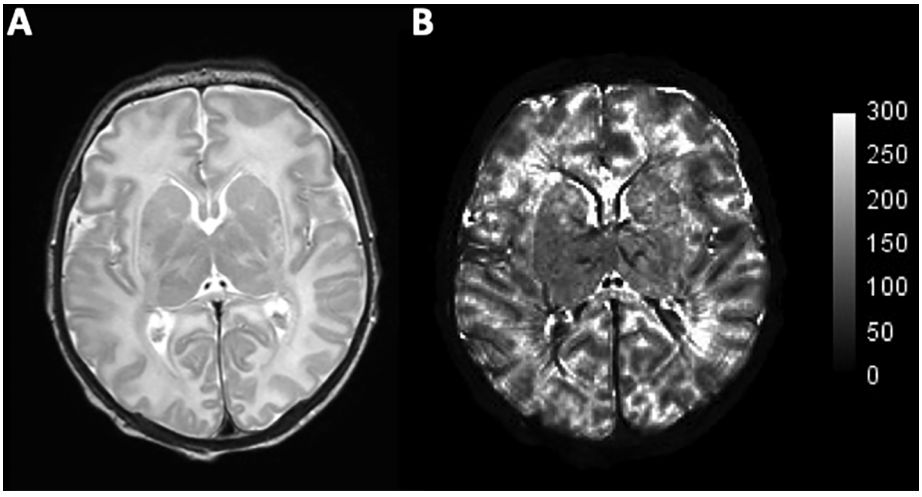

Fig. 2. (A) Axial T2-weighted imaging and (B) axial T2* map (ms) of a neonate with NE treated with hypothermia with brain injury on the brain MRI performed on day 13 of life. Bilateral thalami and bilateral lentiform nuclei are involved, with an increased T2 signal of the supratentorial white matter.

analysis, we did not apply a multiplicity adjustment.

No official sample size calculation was conducted; the included sample was a sample of convenience based on a feasibility assessment.

Statistical significance was set *a priori* at p value < *0.05*. We conducted statistical analyses using SPSS version 24.0 (IBM, Armonk, NY, USA).

3. Results

3.1. Patients

We obtained a total of 74 MRI scans over the first month of life for six healthy neonates, 17 neonates with NE who were treated with hypothermia and did not develop brain injury (Fig. 1), and 16 neonates with NE who were treated with hypothermia and developed brain injury (Fig. 2). Brain injury included basal ganglia injury (44%; 7/16), watershed injury (6%; 1/16), and near-total injury (50%; 8/16).

The 33 neonates with NE had a total of 68 scans over the first month of life: 64% (21/33) had a MRI scan on day 2 of life, 85% (28/33) had a MRI scan around day 10 of life (mean [95% CI]: 11.6 [11.2–12.1]), and 58% (19/33) had a MRI scan around day 30 of life (mean [95% CI]: 32.4 [30.4–34.3]). The six healthy neonates had a total of six scans performed over the first month of life: 17% (1/6) had a MRI scan on day 10 of life, and 83% (5/6) had a MRI scan around day 30 of life (mean [95% CI]: 35.4 [23.8–47.0]).

The 33 neonates with NE had a mean gestational age of 39.16 weeks (95% CI: 38.57–39.74). The six healthy neonates had a mean gestational age of 38.73 weeks (95% CI: 37.82–39.64). Gestational age, birth weight, sex, mode of delivery, Apgar score ≤ 5 at 10 min of life, arterial cord pH and hemoglobin on day two of life were not different for the neonates with brain injury and the neonates without brain injury (i.e., healthy neonates and asphyxiated neonates without injury) (Table 1).

3.2. Analysis of T2* according to the MRI timing

When comparing the neonates with NE who developed injury to the neonates without injury according to the MRI timing, T2* significantly increased in the posterior limbs of the internal capsule on day two of life ($p < 0.001$), around day 10 of life ($p < 0.001$), and around day 30 of life ($p < 0.001$) (Table 2). T2* significantly increased in the thalami on day two of life ($p = 0.001$), around day 10 of life ($p = 0.006$), and around day 30 of life ($p = 0.016$). T2* significantly increased in the lentiform nuclei only on day two of life ($p = 0.005$) (Table 2), with no difference around day 10 or day 30 of life. T2* significantly increased in the anterior (day two of life: $p = 0.002$; day 10 of life: $p = 0.006$; and day 30 of life: $p = 0.002$) and posterior (day two of life: $p = 0.001$; and day 10 of life: $p = 0.008$; and day 30 of life: $p = 0.03$) white matter (Table 2). T2* significantly increased on day two of life ($p = 0.01$) and around day 10 of life ($p = 0.006$) in the genu of the corpus callosum (Table 2), with no difference in this region of interest around day 30 of life. We did not find a significant difference in T2* in the splenium of the corpus callosum across all the time-points. T2* significantly increased around day 30 of life ($p < 0.001$) in the optic radiations (Table 2), with no difference on day two or around day 10 of life.

3.3. Analysis of T2* according to the post-menstrual age at the time of the MRI

When comparing the T2* according to the post-menstrual age at the time of the MRI for the neonates without injury, we found a moderate correlation between the T2* values and the post-menstrual gestational age at the time of the MRI in the thalamus (r = -0.451; $p < 0.0001$) (Fig. 3); we also found a weak correlation in the posterior limbs of the internal capsule (r = -0.334; $p = 0.002$), the lentiform nuclei (r = -0.259; $p = 0.021$), the genu of the corpus callosum (r = -0.296; $p = 0.003$), and the optic radiations (r = -0.240; $p = 0.015$) (Figs. 3 and 4). We did not

Table 1
Clinical characteristics of the study patients.

	NBI			BI	$\Delta_{NBI\text{-}BI}$ (95% CI)*
	Healthy neonates (n = 6)	Neonates with NE treated with hypothermia not developing brain injury (n = 17)	Total NBI (n = 23)	Neonates with NE treated with hypothermia developing brain injury (n = 16)	
Gestational age (week), mean (95% CI)	38.73 (37.82, 39.64)	38.99 (38.12, 39.86)	38.92 (38.27, 39.57)	39.33 (38.45, 40.21)	−0.41 (−1.44, 0.63)
Birth weight (gram), mean (95% CI)	3390 (3146, 3634)	3544 (3215, 3873)	3504 (3261, 3746)	3339 (3023, 3655)	165 (−214, 543)
Sex					
Male, n (%)	4 (67)	10 (59)	14 (61)	10 (63)	−2 (−29, 28)
Female, n (%)	2 (33)	7 (41)	9 (39)	6 (37)	
Mode of delivery					
Vaginal delivery, n (%)	5 (83)	10 (59)	15 (65)	11 (69)	−4 (−30, 26)
Cesarean section, n (%)	1 (17)	7 (41)	8 (35)	5 (31)	
Apgar score ≤ 5 at 10 min, n (%)	0 (0)	10 (59)	10 (43)	12 (75)	−32 (−55, 0.1)
Arterial cord pH, mean (95% CI)	7.31 (7.24, 7.38)	6.99 (6.86, 7.12)	7.06 (6.94, 7.18)	7.00 (6.89, 7.11)	0.06 (−0.10, 0.22)
First gas pH, mean (95% CI)	n/a	7.06 (6.99, 7.12)		6.99 (6.91, 7.07)	
Modified Sarnat score on admission to the neonatal intensive care unit					
1, n (%)	n/a	1 (6)		1 (6)	
2, n (%)	n/a	13 (76)		12 (75)	
3, n (%)	n/a	3 (18)		3 (19)	
Hemoglobin on day 2 of life (g/L), mean (95% CI)	171.00 (69.35, 272.65)	153.59 (146.17, 161.01)		155.42 (148.23, 162.61)	145.81 (131.72, 159.90)	9.61 (−4.86, 24.07)

Abbreviations: BI, brain injury; CI, confidence interval; Δ, difference; NBI, no brain injury (i.e., healthy neonates and asphyxiated neonates without injury); NICU, neonatal intensive care unit
*Note: $\Delta_{NBI\text{-}BI}$ (95% CI), contrasting BI vs. NBI, are presented only for variables with available data in both NBI subgroups (healthy neonates and neonates with NE treated with hypothermia not developing brain injury)

Table 2
T2* values over time adjusted for gestational age in each brain region of interest. Mean (95% CI), unit: ms. Lower values reflect increased myelin content.

		DOL2	DOL10	DOL30
PLIC	**NBI**	117.5 (109.2–125.8)	101.9 (96.7–107.1)	103.3 (98.8–107.8)
	BI	140.5 (131.1–150.0)	119.4 (112.8–126.0)	114.8 (109.7–119.8)
	***p* value ***	***<0.001***	***<0.001***	***0.001***
Thalamus	**NBI**	120.4 (114.2–126.5)	112.4 (106.8–117.9)	109.9 (105.5–114.3)
	BI	135.8 (129.4–142.3)	124.5 (117.8–131.2)	117.9 (113.1–122.6)
	***p* value ***	***0.001***	***0.006***	***0.016***
Lentiform nucleus	**NBI**	113.3 (106.3–120.2)	115.3 (108.2–122.5)	111.3 (105.7–116.9)
	BI	128.5 (120.4–136.5)	119.1 (110.6–127.7)	114.5 (108.4–120.6)
	***p* value ***	***0.005***	*ns*	*ns*
Anterior white matter	**NBI**	175.0 (159.1–190.9)	185.5 (172.1–198.8)	169.8 (153.0–186.6)
	BI	219.6 (197.0–242.3)	227.6 (200.8–254.5)	223.8 (193.7–254.0)
	***p* value ***	***0.002***	***0.006***	***0.002***
Posterior white matter	**NBI**	167.4 (150.4–184.4)	174.0 (159.7–188.3)	148.5 (133.3–163.6)
	BI	219.5 (194.5–244.5)	216.6 (188.6–244.6)	181.1 (155.9–206.2)
	***p* value ***	***0.001***	***0.008***	***0.030***
Genu of corpus callosum	**NBI**	135.0 (126.7–143.2)	132.7 (120.7–144.7)	133.3 (121.2–145.4)
	BI	155.7 (142.4–169.1)	177.3 (148.6–206.1)	154.6 (133.6–175.6)
	***p* value ***	***0.010***	***0.006***	*ns*
Splenium of corpus callosum	**NBI**	138.2 (126.8–149.6)	125.3 (112.1–138.5)	125.6 (117.1–134.1)
	BI	133.4 (117.2–149.6)	147.6 (119.9–175.3)	132.8 (118.0–147.5)
	***p* value ***	*ns*	*ns*	*ns*
Optic radiation	**NBI**	125.8 (118.1–133.5)	142.1 (134.9–149.3)	124.9 (119.2–130.7)
	BI	129.0 (118.9–139.1)	148.9 (135.3–162.4)	149.9 (140.1–159.7)
	***p* value ***	*ns*	*ns*	***<0.001***

* Comparison BI vs. NBI after sequential Sidak correction.
Abbreviations: DOL, day of life, NBI, no brain injury (i.e., healthy neonates and asphyxiated neonates without injury); BI, brain injury; ns, not significant.

find a correlation between the two parameters for the anterior/posterior white matter and the splenium of the corpus callosum. With respect to the neonates with NE who developed injury, we found a moderate correlation in the posterior limbs of the internal capsule (r = -0.415; $p = 0.001$), the thalami (r = -0.525; $p < 0.0001$) (Fig. 3), and the posterior white matter (r = -0.462; $p = 0.004$) (Fig. 4); and we found a weak correlation between the T2* values and the post-menstrual gestational age at the time of the MRI in the lentiform nuclei (r = -0.272; $p = 0.035$) (Fig. 3). We did not find a correlation between the two parameters for the anterior white matter, the genu and splenium of the corpus callosum, and the optic radiations. Interestingly, the T2* values for the neonates with NE who developed injury appeared to reach the same values observed in the neonates without injury around 45–47 weeks of post-menstrual gestational age with respect to the thalamus and the posterior white matter.

4. Discussion

The myelination process (i.e., the production of myelin sheaths to encapsulate axons in the nervous system) is a crucial brain maturational process that enables the proper functioning of neurons and maintains the structural integrity of the connections in the brain (Saab et al., 2013; Yeung et al., 2014). Assuming that myelin is the main contributing factor to the T2* measurements in the neonatal brain (Baxan et al., 2010; Kucharczyk et al., 1994; Stanisz et al., 1999; Henkelman et al., 1993; Lee et al., 2012; Liu et al., 2011; Ning et al., 2014; O'Brien and Sampson, 1965; Zhong et al., 2011), our study confirms the results of previous histopathological studies that have shown that the posterior limbs of the internal capsule, the thalami, and the lentiform nuclei are being actively myelinated around the time of term birth and in the month following birth (Hasegawa et al., 1992; Kinney et al., 1988; Usagre, 2012). Indeed, we have correlated the myelination in the posterior limbs of the internal

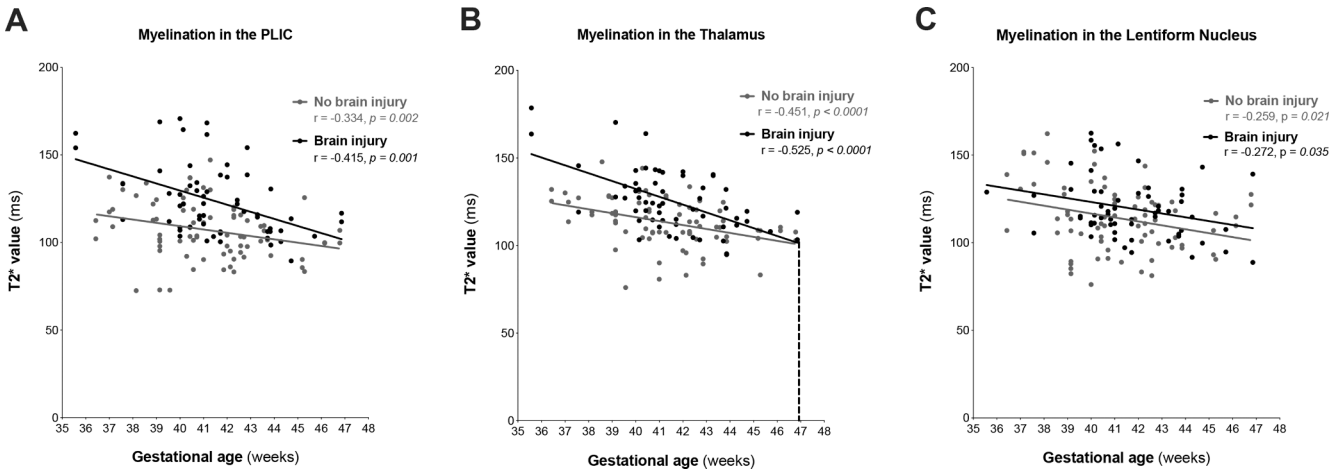

Fig. 3. Correlation between the T2* values (ms) reflecting myelination and the post-menstrual age at the time of the MRI (A) in the posterior limb of the internal capsule (PLIC), (B) in the thalamus, and (C) in the lentiform nucleus. Spearman correlations.

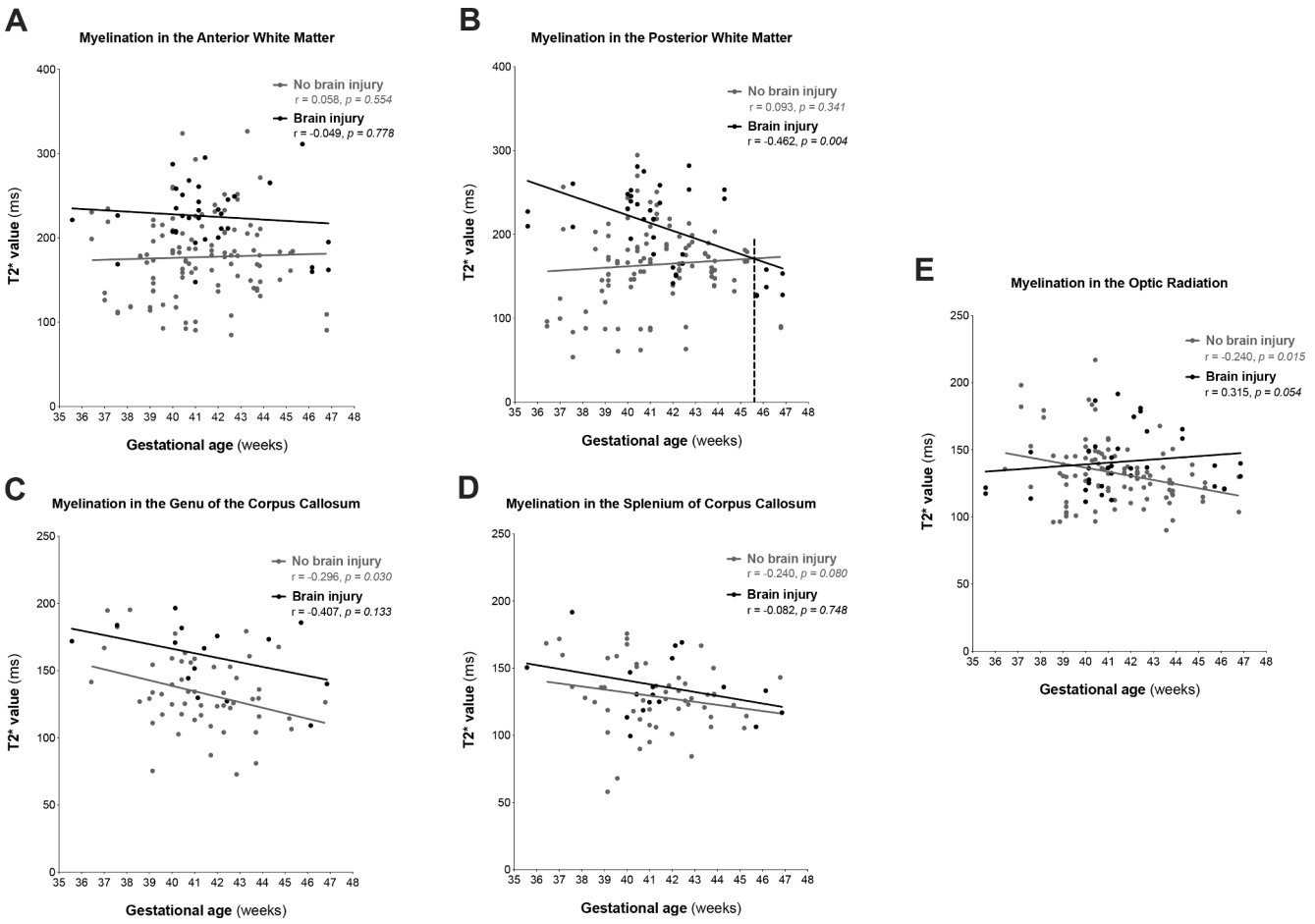

Fig. 4. Correlation between the T2* values (ms) reflecting myelination and the post-menstrual age at the time of the MRI (A) in the anterior white matter, (B) in the posterior white matter, (C) in the genu of the corpus callosum, (D) in the splenium of the corpus callosum, and (E) in the optic radiations. Spearman correlations.

capsule, the thalami, and the lentiform nuclei with the post-menstrual age of the neonates without injury at the time of the MRI over the first month of life. In addition, our study highlights that brain injury secondary to birth asphyxia may impair myelination over the first month of life in those brain regions that are myelinated at birth or soon after birth. Interestingly, our results seem to indicate that the impaired myelination observed in the thalami recovered over time (by 47 weeks of post-menstrual gestational age), which suggests that these impairments may be a *delay* in myelination rather than a permanent interruption of the process in the neonates with NE who developed brain injury, despite hypothermia treatment. This would be in line with previous studies, in which premature infants with brain injury displayed a similar delay in myelination compared to healthy term infants (van de Bor et al., 1989). These studies hypothesized that the brain injury affected the oligodendrocytes significantly enough so that these cells could no longer produce myelin at the typical rate, which caused these neonates to suffer from a delay in myelination at 44 weeks postmenstrual age (van de Bor et al., 1989). Similar mechanisms may be at play in near-term/term neonates with NE, whereby the brain injury caused by birth asphyxia may disturb the ability of the oligodendrocytes to produce myelin at a regular rate, which may cause a delay in myelination. It also remains to be determined whether these initial myelination impairments eventually translate into reduced neuron functioning or contribute to long-term neurodevelopmental impairments when these neonates grow up.

In the neonates without injury, T2* was not correlated with the post-menstrual age at the time of the MRI in the other regions of interest, except for the genu of the corpus callosum and the optic radiations where T2* appears to start decreasing by the end of the first month of life. Again, this finding is in accordance with previous histopathological studies that have shown that these brain regions are being myelinated only months after term birth (Kinney et al., 1988; Hasegawa et al., 1992; Usagre, 2012). For example, the corpus callosum is known to be myelinated by around 4 months after term birth (Kinney et al., 1988; Poduslo and Jang, 1984), and the myelination of the optic radiations appears to start around 1 month of life and completes around 7 months after birth (Dubois et al., 2008; Deoni et al., 2011; Hasegawa et al., 1992). Interestingly, brain injury secondary to birth asphyxia also impairs myelination around day 30 of life in the optic radiations — at the time when myelination appears to start in the neonates without injury — which suggests that an event at birth may still impact myelination in the regions where this process starts only after the perinatal period. Brain injury secondary to birth asphyxia also impairs myelination over the first month of life in the anterior and posterior white matter where myelination does not occur until months after birth, which could suggest that the oligodendrocytes responsible for myelination in the white matter in the central nervous system may be directly injured after birth asphyxia as described in the animal models of this condition (Deng et al., 2014; Guadagno et al., 2015; Li et al., 2017; Wyatt, 2007; Xie et al., 2016). Brain injury secondary to birth asphyxia impairs myelination only on day 10 in the genu of the corpus callosum where myelination does not usually occur until months after birth, and where brain injuries are attributed typically to Wallerian degeneration (Neil and Inder, 2006; Righini et al., 2010). Therefore, it is not possible to determine, from our results, whether the myelination of these structures will be impaired in the neonates with NE who develop brain injury, or whether these impairments could potentially recover over time. Thus, it would be

important for future studies to monitor the T2* measurements for the neonates with NE beyond the first month of life, since the impact of birth asphyxia on myelination may only be appreciated later and may contribute to later abnormal neurodevelopment outcomes (Poduslo and Jang, 1984; van Der Knapp et al., 1991; Paus et al., 2001; Mathur et al., 2010).

To our knowledge, the present study is the first study to investigate myelination over the first month of life using a T2* mapping sequence for healthy neonates and neonates with NE who were treated with hypothermia. Previous studies of neonatal myelination were based mainly on histopathological studies of autopsied neonates (Gilles, 1976; Brody et al., 1987; Kinney et al., 1988; Hasegawa et al., 1992). However, the advent of MR imaging has enabled the evaluation of myelination *in vivo* (Barkovich et al., 1998; Deoni et al., 2011; Huntenburg et al., 2017). Previously, several MRI techniques have been used to assess myelination in adults and children, but most of them have not studied neonates within the first month of life (Barkovich et al., 1998; Deoni et al., 2011; Iwatani et al., 2015; Huntenburg et al., 2017). Among the different techniques available to assess myelination, the contrast between white and grey matter using T1-weighted and T2-weighted imaging has been used (Barkovich et al., 1998; Hasegawa et al., 1992), but this method, which relies on a qualitative comparison, is not optimal for visualizing all the stages of myelination, and does not quantify myelination. The early stages of myelination (*pre-myelination*) are better visualized using T1-weighted imaging, whereas the later stages of myelination (thought to correspond to the maturation of the myelin sheath) are better visualized using T2-weighted imaging (Welker and Patton, 2012; Dubois et al., 2014). The T1- and T2-weighted MRI ratio is another approach that has been used to assess myelination (Glasser and Van Essen, 2011; Soun et al., 2017). Soun et al., (2017) have described ratio intensity values in 10 term neonates without injury and have suggested that these values may be susceptible to hyperintensities, such as those present in neonates with NE who develop injury.

Diffusion-tensor imaging (DTI) is a commonly used method for imaging white matter fiber tracts in the human brain, based on the principle that the diffusion of water molecules found in brain tissues is restricted by the local microstructure (Huppi et al., 1998; Neil et al., 2002; Partridge et al., 2004; Dubois et al., 2014). Various studies have suggested that myelin content indirectly affects the anisotropy of diffusion, with areas containing less myelinated axons showing less diffusion anisotropy (Alexander et al., 2007). However, other studies have cautioned against the use of DTI and radial diffusivity to assess myelin (Wheeler-Kingshott and Cercignani, 2009).

Magnetization transfer is another technique regularly used to study myelin. In its simplest form, a magnetization transfer ratio (MTR) is estimated as a semi-quantitative marker of myelination in the brain (Kucharczyk et al., 1994; McGowan, 1999; Dubois et al., 2014; Fjær et al., 2015). The ratio between the free and bound water molecules is thought to represent the myelin content during axonal myelination (Kucharczyk et al., 1994). However, some studies also have pointed to the controversial results obtained by using a magnetization transfer ratio to quantify myelination (Fjær et al., 2015; Serres et al., 2009, 2013). One of these studies has demonstrated that magnetization transfer ratio values were inaccurate in describing myelination in an experimental mouse model of autoimmune encephalomyelitis, characterized by lymphocyte-mediated inflammation followed by demyelination, axonal degeneration, and neuronal loss; and did not correlate with the histopathological myelin content (Fjær et al., 2015). These results, and those of other previous studies, suggest that the magnetization transfer ratio technique may be more sensitive to inflammatory processes and less sensitive to myelination and demyelination processes (Serres et al., 2009, 2013; Fjær et al., 2015). Other more sophisticated magnetization transfer techniques such as quantitative magnetization transfer (qMT) (Henkelman et al., 1993) and inhomogeneous magnetization transfer (ihMT) (Varma et al., 2015) are likely to be more specific to myelin. However, they typically require long acquisition sequences, are not widely available, and can lead to a high specific absorption rate (SAR), which can be problematic when imaging neonates.

Another imaging technique that has shown good specificity for myelin is myelin water imaging (MWI), which obtains a myelin water fraction (MWF) by estimating the short-T2 component of the water T2 relaxation-time spectrum. Recently, this technique has been applied to neonatal imaging (Webber et al., 2019), but one important downside is the comparatively low signal-to-noise ratio, which makes imaging a challenge with respect to the low myelin concentration found in the neonatal brain. MWF also can be estimated using an approach based on multi-component relaxation (MCR) (Deoni et al., 2011; Dubois et al., 2014). This technique attempts to break down the MR signal into its different component parts (i.e., different tissues will exhibit different relaxation times), which can be parcellated by multi-component relaxation analyses (Deoni et al., 2011). Three studies by Dean et al., 2016, Deoni et al., 2011, Deoni et al., 2012 have used a new multi-component relaxation technique known as multicomponent driven equilibrium single pulse observation of T1 and T2 (McDESPOT) to quantify myelin levels in healthy infants between 3 months of age and 7.5 years. Despite its higher resolution, this approach is not optimal with neonatal populations due to its longer scan times (Soun et al., 2017), which makes it more difficult to add to the baseline MRI protocol in a population of critically ill neonates. Concerns also have been raised recently regarding the accuracy of the technique (West et al., 2019).

The differences in the susceptibility of myelin and most other water-based tissues lead to signal intensity loss in T2*-weighted imaging, which makes brain regions with higher levels of myelin content appear darker on T2*-weighted images (Chavhan et al., 2009). Although susceptibility and T2*-based techniques have been used mainly until now to detect calcium depositions, to measure iron content, and to image haemorrhagic infarcts in adults (Li et al., 1998, 2009; Wu et al., 2010), many studies have demonstrated that myelin content is the main contributor to T2* decay (Baxan et al., 2010; Henkelman et al., 1993; Kucharczyk et al., 1994; Lee et al., 2012; Liu et al., 2011; Ning et al., 2014; O'Brien and Sampson, 1965; Stanisz et al., 1999; Zhong et al., 2011), especially in neonates who are less likely to have a high concentration of iron and calcium. In fact, despite the multifactorial nature of the T2* signal, several studies have shown that myelin content may be the main contributor to the signal (Baxan et al., 2010; Henkelman et al., 1993; Kucharczyk et al., 1994; Lee et al., 2012; Liu et al., 2011; Ning et al., 2014; O'Brien and Sampson, 1965; Stanisz et al., 1999; Zhong et al., 2011). Using a mouse model of cuprizone-induced demyelination, Lee et al., (2012) established a direct link between T2* decay and myelin content. This type of MR imaging has demonstrated multiple advantages for quantifying myelination over other previously discussed techniques. It has a good signal-to-noise ratio (SNR) and a short scanning time of <4 min (Hwang et al., 2010), and thus can be added more easily to the baseline protocol for imaging healthy and critically ill neonates. While T2* is also known to be influenced by white matter orientation effects (Lee et al., 2011), the fact that the neonates were all immobilized in a similar position and that the same regions of interest were accessed for all subjects likely decreased the impact on this confounding factor on the results. A variation of this technique that enhanced T2*-weighted angiography (ESWAN) by focusing on R2* values ($R2^* = 1/T2^*$) has been used to evaluate myelin content in healthy infants born at term who were around 3 months of age at the time of the MRI (Ning et al., 2014), and this study demonstrated, similar to the present study, that the R2* values in the grey nuclei and white matter were correlated with postmenstrual age (Ning et al., 2014).

The strength of the current study is the serial MRI design that followed the evolution of myelination over time during the first month of life of neonates with NE who were treated with hypothermia. The main limitation of the present study is that only six healthy neonates were included, which did not enable us to do a sub-analysis to rule out a potential difference in the myelination of the neonates with NE without injury, compared to the healthy neonates. For our study, we assumed

that if a neonate with NE did not develop brain injury, he/she should not have myelination abnormalities, and thus we grouped them together as neonates without injury; however, a study with a larger sample size (especially of healthy neonates) would be needed to confirm this assumption. In addition, the healthy neonates were not imaged on day two of life, only later, which made it impossible to confirm from our data that the hypothermia treatment did not influence the myelination values on day two of life. Our study also compared the myelination of the neonates with and without injury only during the first month of life, although the myelination process continues well beyond this first month. Thus, future studies should investigate how myelination evolves in these critically ill neonates after the first month of life, and whether the initial asphyxial event continues to impair this process after birth. It also would be important to investigate how these myelination impairments correlate with adverse long-term neurological development. Although our study assessed myelination in eight regions of interest, future studies may want to focus on other regions (e.g., the cerebellar peduncles, the rostrum, the body of the corpus callosum, etc.).

In conclusion, birth asphyxia may impair myelination in brain regions that are typically myelinated at birth or soon thereafter (the posterior limbs of internal capsule, the thalami, and the lentiform nuclei), in brain regions where the myelination process begins only after the perinatal period (the optic radiations), and in brain regions where this process does not occur until months after birth (the anterior/posterior white matter), in addition to causing the well-described direct injury to the brain. Future studies should aim to confirm whether these impairments are temporary or persistent, and how they correlate with long-term neurodevelopmental impairments. It also would be of the utmost importance to perform similar studies with these critically ill neonates beyond the first month of life to examine how the brain regions that are being myelinated only several months after birth are being affected by the initial asphyxial event.

Declaration of Competing Interest

This manuscript has been contributed to, seen, and approved by all the authors. All the authors fulfill the authorship criteria requirements. No conflict of interest exists. Guillaume Gilbert is an employee of Philips Healthcare. The authors have no financial relationships relevant to this article to disclose. Bianca Olivieri received research grant funding from McGill University's G.R. Caverhill Fellowship for this work. Pia Wintermark receives research grant funding from the FRSQ Clinical Research Scholar Career Award Junior 2 and a CIHR Project Grant.

Acknowledgments

We thank the families and their neonates for participating in our study. Special thanks also are expressed to the nurses and respiratory therapists from the neonatal intensive care unit, and MRI technicians who have made this study possible. We also thank Mr. Wayne Ross Egers for his professional English correction of our study.

References

Al Amrani, F., Marcovitz, J., Sanon, P.N., Khairy, M., Saint-Martin, C., Shevell, M., Wintermark, P., 2018. Prediction of outcome in asphyxiated newborns treated with hypothermia: is MRI scoring system described before the cooling era still useful? Eur. J. Paediatr. Neurol. 22, 387–395.

Alexander, A.L., Lee, J.E., Lazar, M., Field, A., 2007. Diffusion tensor imaging of the brain. Neurotherapeutics 4, 316–329.

Al-Macki, N., Miller, S.P., Hall, N., Shevel, M., 2009. The spectrum of abnormal neurologic outcomes subsequent to term intrapartum asphyxia. Pediatr. Neurol. 41, 399–405.

Barkovich, A.J., Kjos, B.O., Jackson, D.E., Norman, D., 1998a. Normal maturation of the neonatal and infant brain: MR imaging at 1.5T. Radiology 166, 173–180.

Barkovich, A.J., Hallam, D., 1997. Neuroimaging in Perinatal Hypoxic-Ischemic Injury. Ment. Retard. Dev. Disabil. 3, 28–41.

Barkovich, A.J., Hajnal, B.L., Vigneron, D., Sola, A., Partridge, J.C., Allen, F., Ferriero, D. M., 1998b. Prediction of neuromotor outcome in perinatal asphyxia: Evaluation of MR scoring systems. Am. J. Neuroradiol. 19, 143–149.

Baxan, N., Harsan, L.A., Dragonu, I., Merkle, A., Henning, J., von Elverfeldt, D., 2010. In: Myelin as a primary source of phase contrast demonstrated in vivo in the mouse brain. Proceedings of the 18th Annual Meeting of ISMRM. Stockholm, Sweden.

Boudes, E., Tan, X., Saint-Martin, C., Shevell, M., Wintermark, P., 2015. Magnetic resonance imaging obtained during versus after hypothermia in asphyxiated newborns. Arch. Dis. Child. Fetal. Neonatal Edition 100, 238–242.

Brody, B.A., Kinney, H.C., Kloman, A.S., Gilles, F.H., 1987. Sequence of central nervous system myelination in human infancy I: an autopsy study of myelination. J. Neuropathol. Exp. Neurol. 46, 283–301.

Bryce, J., Boschi-Pinto, C., Shibuya, K., Black, R.E., WHO Child Health Epidemiology Reference Group, 2005. WHO estimates of the causes of death in children. Lancet. 365, 1147–1152.

Cabaj, A., Bekiesinski-Figatowska, M., Madzik, J., 2012. MRI Patterns of Hypoxic-Ischemic Brain Injury in Preterm and Full Term Infants – Classical and Less Common MRI Findings. Polish J. Radiol. 77, 61–76.

Chavhan, G.B., Babyn, P.S., Thomas, B., Schroff, M., Haacke, E.M., 2009. Principles, techniques, and applications of T2*-based MR imaging and its special applications. Radiographics 29, 1433–1449.

Dean 3rd, D.C., O'Muircheartaigh, J., Dirks, H., Travers, B.G., Adluru, N., Alexander, A. L., Deoni, S.C.L., 2016. Mapping an index of the myelin g-ratio in infants using magnetic resonance imaging. Neuroimage 132, 225–237.

Deng, Y., Xie, D., Fang, M., Zhu, G., Chen, C., Zeng, H., Lu, J., Charanjit, K., 2014. Astrocyte-derived proinflammatory cytokines induce hypomyelination in the periventricular white matter in the hypoxic neonatal brain. PLoS ONE.

Deoni, S.C.L., Mercure, E., Blasi, A., Gasston, D., Thomson, A., Johnson, M., Williams, S. C.R., Murphy, D.G.M., 2011. Mapping infant brain myelination with magnetic resonance imaging. J. Neurosci. 31, 784–791.

Deoni, S.C., Dean 3rd, D.C., O'Muircheartaigh, J., Dirks, H., Jerskey, B.A., 2012. Investigating white matter development in infancy and early childhood using myelin water faction and relaxation time mapping. Neuroimage 63, 1038–1053.

Ding, X.Q., Sun, Y., Braass, H., Illies, T., Zeumer, H., 2008. Evidence of rapid ongoing brain development beyond 2 years of age detected by fiber tracking. Am. J. Neuroradiol. 29, 1261–1265.

Dubois, J., Dehaene-Lambertz, G., Kulikova, S., Poupon, C., Hüppi, P.S., Hertz-Pannier, L., 2014. The early development of brain white matter: a review of imaging studies in fetuses, newborns and infants. Neuroscience 276, 48–71.

Dubois, J., Dehaene-Lambertz, G., Perrin, M., Mangin, J.F., Cointepas, Y., Duchesnay, E., le Bihan, D., Hertz-Pannier, L., 2008. Asynchrony of the early maturation of white matter bundles in healthy infants: quantitative landmarks revealed noninvasively by diffusion tensor imaging. Hum. Brain Mapp. 29, 14–27.

Fatemi, A., Wilson, M.A., Johnston, M.V., 2009. Hypoxic-ischemic encephalopathy in the term infant. Clin. Perinatol. 36, 835–858.

Ferriero, D.M., 2004. Neonatal brain injury. N. Engl. J. Med. 351, 1985–1995.

Fjær, S., Bø, L., Myhr, K.M., Tirkildsen, Ø., Wergeland, S., 2015. Magnetisation transfer ratio does not correlate to myelin content in the brain in the MOG-EAE mouse model. Neurochem. Int. 83–84, 28–40.

Gilles, F., 1976. Myelination in the neonatal brain. Hum. Pathol. 7, 244–248.

Glasser, M.F., Van Essen, D.C., 2011. Mapping human cortical areas in vivo based on myelin content as revealed by T1- and T2-weighted MRI. J. Neurosci. 31, 11597–11616.

Gold, B.T., Johnson, N.F., Power, D.K., Smith, C.D., 2012. White matter integrity and vulnerability to Alzheimer's disease: preliminary findings and future directions. BBA 1822, 416–422.

Grodd, W., 1993. Normal and abnormal patterns of myelin development of the fetal and infantile human brain using magnetic resonance imaging. Curr.Opin. Neurol. Neurosurgery 6, 393–397.

Guadagno, J., Swan, P., Shaikh, R., Cregan, S.P., 2015. Microglia-derived IL-1β triggers p53-mediated cell cycle arrest and apoptosis in neural precursor cells. Cell Death Dis. 6.

Hasegawa, M., Houdou, S., Mito, T., Takashima, S., Asanuma, K., Ohno, T., 1992. Development of myelination in the human fetal and infant cerebrum: a myelin basic protein immunohistochemical study. Brain Development 14, 1–6.

Henkelman, R.M., Huang, X., Xiang, Q.S., Stanisz, G.J., Swanson, S.D., Bronskill, M.J., 1993. Quantitative interpretation of mangetization transfer. Magn. Reson. Med. 29, 759–766.

Holland, B.A., Haas, D.K., Norman, D., Brant-Zawadzki, M., Newton, T.H., 1986. MRI of normal brain maturation. Am. J. Neuroradiol. 7, 201–208.

Huang, B.Y., Castillo, M., 2008. Hypoxic-Ischemic Brain Injury: Imaging Findings from Birth to Adulthood. Radiographics 28, 417–439.

Huntenburg, J.M., Bazin, P.L., Goulas, A., Tardif, C.L., Villringer, A., Margulies, D.S., 2017. A systematic relationship between functional connectivity and intracortical myelin in the human cerebral cortex. Cereb. Cortex 27, 981–997.

Huppi, P.S., Maier, S.E., Peled, S., Zientara, G.P., Barnes, P.D., Jolesz, F.A., Vole, J.J., 1998. Microstructural development of human newborn cerebral white matter assessed in vivo by diffusion tensor magnetic resonance imaging. Pediatr. Res. 44, 584–590.

Hwang, D., Kim, D.H., Du, Y.P., 2010. In vivo multi-slice mapping of myelin water content using T2* decay. NeuroImage 52, 198–204.

Iwatani, J., Ishida, T., Donishi, T., Ukai, S., Shinosaki, K., Terada, M., Kaneoke, Y., 2015. Use of T1-weighted/T2-weighted magnetic resonance ratio images to elucidate changes in the schizophrenic brain. Brain and Behaviour 5, 1–14.

Kinney, H.C., Brody, B.A., Kloman, A.K., Gilles, F.H., 1988. Sequence of central nervous system myelination in human infancy II: Patterns of Myelination in Autopsied Infants. J. Neuropathol. Exp. Neurol. 47, 217–234.
Kucharczyk, W., Macdonald, P.M., Stanisz, G.J., Henkelman, R.M., 1994. Relaxivity and magnetization transfer of white matter lipids at MR imaging: importance of cerebrosides and pH. Radiology 192, 521–529.
Lee, J., van Gelderen, P., Kuo, L.W., Merkle, H., Silva, A.C., Duyn, J.H., 2011. T2*-based fiber orientation mapping. Neuroimage 57, 225–234.
Lee, J., Shmueli, K., Kang, B.T., Yao, B., Fukanaga, M., van Gelderen, P., Palumbo, S., Bosetti, F., Silva, A.C., Duyn, J.H., 2012. The contribution of myelin to magnetic susceptibility-weighted contrasts in high-field MRI of the brain. Neuroimage 59, 3967–3975.
Li, B., Concepcion, K., Meng, X., Zhang, L., 2017. Brain-immune interactions in perinatal hypoxic-ischemic brain injury. Prog. Neurobiol. 159, 50–68.
Li, D., Wright, D.J., Wang, Y., 1998. In vivo correlation between blood T2* and oxygen saturation. J. Magn. Reson. Imaging 8, 1236–1239.
Li, T.Q., van Gelderen, P., Merkel, H., Dodd, S., Talagala, L., Koretsky, A.P., Duyn, J., 2009. Characterisation of T2* Heterogeneity in Human Brain White Matter. Magn. Reson. Med. 62, 1652–1657.
Liu, C., Li, W., Johnson, G.A., Wu, B., 2011. High-field MRI of brain dysmyelination by quantitative mapping of magnetic susceptibility. Neuroimage 56, 930–938.
Mathur, A.M., Neil, J.J., Inder, T.E., 2010. Understanding brain injury and neurodevelopmental disabilities in the preterm infant: the evolving role of advanced MRI. Semin Perinatology 34, 57–66.
McGowan, J.C., 1999. The physical basis of magnetization transfer imaging. Neurology 53, S3–S7.
Nave, K.A., Bruce, T.D., 2008. Axon-glial signaling and the glial support of axon function. Annu. Rev. Neurosci. 31, 535–561.
Neil, J., Miller, J., Mukherjee, P., Huppi, P.S., 2002. Diffusion tensor imaging of normal and injured developing human brain—a technical review. NMR Biomed. 15, 543–552.
Neil, J.J., Inder, T.E., 2006. Detection of wallerian degeneration in a newborn by diffusion magnetic resonance imaging (MRI). J Child Neurology 21, 115–118.
Ning, N., Zhang, L., Gao, J., Zhang, Y., Ren, Z., Niu, G., Day, Y., Wu, E.X., Guo, Y., Yang, J., 2014. Assessment of iron deposition and white matter maturation in infant brains using enhanced T2 star weighted angiography: R2* versus phase values. PLoS ONE 9, 1–11.
O'Brien, J.S., Sampson, E.L., 1965. Lipid composition of the normal human brain: gray matter, white matter, and myelin. J. Lipid Res. 6, 537–544.
O'Rahilly, R., Muller, F., 1999. Minireview: summary of the initial development of the human nervous system. Teratology 60, 39–41.
Partridge, S.C., Mukherjee, P., Henry, R.G., Miller, S.P., Berman, J.I., Jin, H., Glenn, O.A., Ferriero, D.M., Barkovich, A.J., Vigneron, D.B., 2004. Diffusion tensor imaging: serial quantitation of white matter tract maturity in premature newborns. Neuroimage 22, 1302–1314.
Paus, T., Collins, D.L., Evans, A.C., Leonard, G., Pike, B., 2001. Maturation of white matter in the human brain: a review of magnetic resonance studies. Brain Res. Bull. 54, 255–266.
Poduslo, S.E., Jang, Y., 1984. Myelin development in infant brain. Neurochem. Res. 9, 1615–1626.
Righini, A., Doneda, C., Parazzini, C., Arrigoni, F., Matta, U., Triulzi, F., 2010. Diffusion tensor imaging of early changes in corpus callosum after acute cerebral hemisphere lesions in newborns. Neuroradiology 52, 1025–1035.
Saab, A.S., Tzetanova, I.D., Nave, K.A., 2013. The role of myelin and oligodendrocytes in axonal energy metabolism. Curr. Opin. Neurobiol. 23, 1065–1072.
Serres, S., Anthony, D.C., Jiang, Y., Campbell, S.J., Broom, K.A., Khrapitchev, A., 2009. Comparison of MRI signatures in pattern i and ii in multiple sclerosis models. NMR Biomed. 10, 1014–1024.
Serres, S., Bristow, C., de Pablos, R.M., Merkler, D., Soto, M.S., Sibson, N.R., 2013. Magnetic resonance imaging reveals therapeutic effects of interferon-beta on cytokine-induced reactivation of rat model of multiple sclerosis. J. Cerebral Blood Flow Metabolism 5, 744–753.
Soun, J., Liu, M.Z., Cauley, K.A., Grinbad, J., 2017. Evaluation of neonatal brain myelination using the T1- and T2-weighted MRI ratio. J. Magn. Reson. Imaging 46, 690–696.
Stanisz, G.J., Kecojevic, A., Bronskill, M.J., Henkelman, R.M., 1999. Characterizing white matter with magnetization transfer and T(2). Magn. Reson. Med. 42, 1128–1136.
Usagre, F.F., 2012. Chronology of normal brain myelination in newborns with MR imaging. ECR 2012.
van de Bor, M., Guit, G.L., Schreuder, A.M., Wondergem, J., Vielvoye, G.J., 1989. Early detection of delayed myelination in preterm infants. Pediatrics 84, 407–411.
Varma, G., Duhamel, G., de Bazelaire, C., Alsop, D.C., 2015. Magnetization transfer from in homogeneously broadened lines: a potential marker for myelin. Magn. Reson. Med. 73, 614–622.
Wang, S., Wu, E.X., Tam, C.N., Lau, H.F., Cheung, P.T., Khong, P.L., 2008. Characterization of White Matter Injury in a Hypoxic-Ischemic Neonatal Rat Model by Diffusion Tensor MRI. Stroke 39, 2348–2353.
Webber, A.M., Zhang, Y., Kames, C., Rauscher, A., 2019. Myelin water imaging and R2* mapping in neonates: investigating R2* dependence on myelin and fibre orientation in whole brain white matter. NMR Biomed. 33.
Welker, K.M., Patton, A., 2012. Assessment of Normal Myelination with Magnetic Resonance Imaging. Semin Neurology 32, 15–28.
West, D.J., Teixeira, R.P.A.G., Wood, T.C., Hajnal, J.V., Tournier, J.D., Malik, S.J., 2019. Inherent and unpredictable bias in multi-component DESPOT myelin water fraction estimation. NeuroImage 195, 78–88.
Wheeler-Kingshott, C.A., Cercignani, M., 2009. About "axial" and "radial" diffusivities. Magn. Reson. Med. 61, 1255–1260.
Wintermark, P., Labrecque, M., Warfield, S.K., DeHart, S., Hansen, A., 2010. Can induced hypothermia be assured during brain MRI in neonates with hypoxic-ischemic encephalopathy? Pediatr. Radiol. 40, 1950–1954.
Wu, G., Xi, G., Hua, Y., Sagher, O., 2010. T2* Magnetic resonance imaging sequences reflect brain tissue iron deposition following intracerebral hemorrhage. Transl Stroke Research 1, 31–34.
Wyatt, J.S., 2007. Mechanisms of brain injury in the newborn. Eye 21, 1261–1263.
Xie, D., Shen, F., He, S., Chen, M., Han, Q., Fang, M., Zeng, H., Chen, C., Deng, Y., 2016. IL-1β induces hypomyelination in the periventricular white matter through inhibition of oligodendrocyte progenitor cell maturation via FYN/MEK/ERK signaling pathway in septic neonatal rats. Glia 62, 583–602.
Yeung, M., Zdunek, S., Bergmann, O., Bernard, O., Salehpour, M., Alkass, K., Peri, S., Tisdale, J., Possnert, G., Brundin, L., Druid, H., Frisen, J., 2014. Dynamics of oligodendrocyte generation and myelination in the human brain. Cell 159, 766–774.
Zhong, K., Ernst, E., Buchthal, S., Speck, O., Anderson, L., Chang, L., 2011. Phase contrast imaging in neonates. Neuroimage 55, 1068–1072.